

Old Dominion University

## ODU Digital Commons

---

Electrical & Computer Engineering Theses & Dissertations

Electrical & Computer Engineering

---

Spring 1994

### Derivative Absorption Spectroscopy with Tunable Laser Diodes

Andrew D. Jackson  
*Old Dominion University*

Follow this and additional works at: [https://digitalcommons.odu.edu/ece\\_etds](https://digitalcommons.odu.edu/ece_etds)



Part of the [Electromagnetics and Photonics Commons](#), and the [Engineering Physics Commons](#)

---

#### Recommended Citation

Jackson, Andrew D.. "Derivative Absorption Spectroscopy with Tunable Laser Diodes" (1994). Master of Science (MS), Thesis, Electrical & Computer Engineering, Old Dominion University, DOI: 10.25777/s414-yw13  
[https://digitalcommons.odu.edu/ece\\_etds/366](https://digitalcommons.odu.edu/ece_etds/366)

This Thesis is brought to you for free and open access by the Electrical & Computer Engineering at ODU Digital Commons. It has been accepted for inclusion in Electrical & Computer Engineering Theses & Dissertations by an authorized administrator of ODU Digital Commons. For more information, please contact [digitalcommons@odu.edu](mailto:digitalcommons@odu.edu).

DERIVATIVE ABSORPTION SPECTROSCOPY WITH  
TUNABLE LASER DIODES

by

Andrew D. Jackson  
B.S.E.E. May 1993, Old Dominion University

A Thesis submitted to the Faculty of  
Old Dominion University in Partial Fulfillment of the  
Requirement for the Degree of

MASTER OF SCIENCE  
ELECTRICAL ENGINEERING

OLD DOMINION UNIVERSITY  
May, 1994

Approved by:

Amin N. Dharamsi (Director)

---

Karl H. Schoenbach

---

Hani Elsayed-Ali

---

## ABSTRACT

### DERIVATIVE ABSORPTION SPECTROSCOPY WITH TUNABLE LASER DIODES

Andrew David Jackson  
Old Dominion University, 1994  
Director: Dr. Amin N. Dharamsi

Derivative Absorption Spectroscopy using tunable diode lasers provides a non-intrusive, sensitive, and convenient method for monitoring gaseous characteristics such as concentration, temperature, and flow velocity. In addition, the specie type can be identified, and if the equation of state is known, pressure may be deduced.

This technique was used on molecular oxygen, in which the rovibronic transitions of the A-band ( $b^1\Sigma_g^+ \leftarrow X^3\Sigma_g^-$ ;  $v''=0, v'=0$ ) were probed. Phase sensitive detection with a lock-in amplifier provides the flexibility to examine lineshape derivatives; several such derivative orders were examined.

The experimental results obtained show excellent agreement with theoretical considerations. The results yield concentration, temperature and collision cross-section.

## ACKNOWLEDGEMENTS

I wish to express my sincere appreciation to a fine mentor--Dr. Amin N. Dharamsi. Without his patience, knowledge, guidance, and belief in the project, I do not believe I could have accomplished this project.

I would also like to express my appreciation to Dr. Roland Mielke and the Electrical and Computer Engineering Department. Through Dr. Mielke's efforts, I was able to begin work on this project and see it through to the end.

I would like to thank the committee for taking the time out of their busy schedules to review and provide constructive criticism of this thesis.

Also, I would like to thank Dr. J. Singh and Greg Herring from NASA-Langley Research Center for their valuable time and guidance throughout this project. Without their efforts, this research could not have been accomplished.

Financial support from a NASA Graduate Research Fellowship (NGT 51103) as well as a Virginia Space Grant Consortium Scholarship is gratefully acknowledged.

Finally, I would like to express my eternal gratitude to my wife, Suanne, for her support and understanding throughout the course of this research.

## TABLE OF CONTENTS

	Page
ACKNOWLEDGEMENTS	ii
TABLE OF CONTENTS	iii
LIST OF FIGURES	v
Chapter	
I. INTRODUCTION	1
II. BACKGROUND	4
Frequency Modulation	5
Frequency Modulation and Derivative Spectroscopy	8
Lineshape Functions	13
Gaussian Profile	14
Lorentzian Profile	15
Voight Profile	17
Our Approximation to the Voight Profile	18
Lineshape Derivatives	19
Concentration and Temperature	25
Concentration	25
Temperature	27

III. EXPERIMENTAL PROCEDURE, RESULTS AND ANALYSIS	32
Experimental Arrangement	32
RQ(11,12) Line Measurements	36
Linewidth Measurements	36
Signal Magnitude	38
Other A-Band Transition Lines	41
Temperature Measurements	46
Higher Order Derivative Measurements	46
IV. APPLICATIONS	50
Gas Concentration Measurements	50
Temperature Measurements	51
Velocity Measurements	51
V. CONCLUSION	53
LIST OF REFERENCES	55

## List of Figures

<u>Figure</u>	<u>Page</u>
1. Fourier Components of a Modulated Diode Laser Beam	7
2. Lorentzian Lineshape and Derivatives	21
3. Gaussian Lineshape and Derivatives	22
4. Oxygen Potential Energy Diagram	28
5. Experimental Apparatus	35
6. (a) Measured FWHM vs. Oxygen Concentration	37
(b) Measured and Calculated FWHM vs. Oxygen Concentration	37
7. (a) Second Harmonic Signal vs. Concentration With Calculated Broadening	40
(b) Second Harmonic Signal vs. Concentration With Theoretical Approximation	40
8. First Derivative Signal of Other A-Band Transitions	42
9. Second Derivative Signal of Other A-Band Transitions	43
10. Other A-Band Transitions	44
11. Other A-Band Transitions	45
12. 1st-5th Derivative Signals	48
13. 2nd-10th Derivative Signals	49

## Chapter I.

### INTRODUCTION

The measurement of gas characteristics is often done in an intrusive fashion. This may be adequate for many applications, but for environments such as wind tunnels, it is desirable to have a non-intrusive, real-time method for measuring quantities such as gas concentration, temperature, and velocity.

The motivation for this research was to provide the NASA-Langley Research Center with a real-time, non-intrusive means for measuring Oxygen concentration and possibly temperature in the eight foot, High-Temperature, Hypersonic Wind Tunnel. Currently, NASA Langley uses a combination of gas chromatography and Zirconium based diffusion sensors to acquire concentration information in the wind tunnel. Although these methods work well, in the gas chromatography method, gas samples are gathered over the entire tunnel test run and an average concentration is measured. In the Zirconium based sensor method, a gas sample is drawn out of the tunnel, and concentrations of oxygen are obtained from concentration gradient data; this sensor provides a signal response on the order of 0.5 s. Neither of these methods provide temperature measurement capabilities, nor are they non-intrusive in nature.

This wind tunnel is used in the design and testing of scramjet engines that will be used in the NASA space plane currently under development. When engine tests are being run, it is of crucial importance that oxygen and other gas concentrations be

monitored and regulated for efficient fuel mixture adjustments. Ideally, the monitoring of the gas concentrations should be non-intrusive in nature so as not to disturb the wind tunnel environment, and should be done in real-time to allow for adjustments during test runs for optimum scramjet performance. Non-intrusive temperature measurements throughout the test run would also be of great value in evaluation of scramjet engine performance. Also, since the wind tunnel is combustion driven, temperature measurements would help in gauging and optimizing the combustion process for maximum wind tunnel efficiency. A method which employs derivative spectroscopy is described in this thesis and provides a good solution for measuring concentration and temperature in a real-time, non-intrusive manner for such an environment.

The general theory behind derivative spectroscopy with tunable diode lasers and the general descriptions of lineshape profiles, broadening mechanisms, and linewidths are discussed. Results obtained by first, second and higher order derivative spectroscopy are given. It is shown that the method provides a very sensitive means for measuring the parameters of interest.

In Chapter II of this thesis, a discussion of the general principles of derivative spectroscopy will be introduced. This discussion will include a general synopsis of lineshape functions, their derivatives and the information that can be extracted from them. This chapter will also include the theory used to extract concentration and temperature for the experiments.

In Chapter III, a discussion of experimental procedures and results will be presented. A detailed description of the experimental arrangement will be given along with a detailed account of the experimental techniques used in this research. Concentration measurements obtained from absorption data for the Oxygen A-band RQ(11,12) transition will be examined. Absorption results obtained from other Oxygen A-band transitions will be given. Higher order lineshape function derivatives will also be offered and the calculation of temperature from derivative absorption profile results obtained from the RQ(11,12) transition will be presented. Chapter III will also compare theoretical results to the experimental data. This will include a discussion of Oxygen concentration and how it affects the experimental results.

Chapter IV will include possible applications for this research. Applications for gas concentration measurements and pollution control will be explored. General temperature measurement applications will be discussed for industrial as well as for research uses. Finally, an application for measuring point velocities will be explored; this is an ideal application for use in aerospace wind tunnels.

Additionally, Chapter V will conclude this thesis, but not the Old Dominion University research into this exciting field of *Derivative Absorption Spectroscopy With Tunable Diode Lasers*.

## **Chapter II.**

### **BACKGROUND**

Derivative spectroscopy using phase sensitive detection is not a new concept. Nuclear Magnetic Resonance experiments using modulated magnetic fields and phase sensitive detection have been around for many years and have been used in experimental studies of weak NMR and ESR studies [7]. Modulation spectroscopy, including derivative spectroscopy, has been reviewed in detail by Cardona [15].

The study of absorption lineshape profiles and linewidths can be made by use of a modulated tunable diode laser and phase sensitive detection. Tunable diode lasers are ideal in the use of derivative spectroscopy because of the low expense and ease of diode modulation. Also, once a system is developed, it almost becomes a turn key operation.

With the advances in laser diode technology, larger portions of the visible and infrared frequency spectra are available for probing transitions with laser diodes. This will enable the investigation of more gas species in the future. Since laser diodes are small and inexpensive, they are ideal for use in space applications and other space limited environments.

The signal to noise ratio for derivative spectroscopy is much greater than for simple direct measurements. Since the transitions probed in this research have sharp

absorption profiles (FWHM on the order of 10 GHz), large derivative absorption signals were easily produced for these very weak absorption lines.

### Frequency Modulation

When a small sinusoidal current of frequency  $\omega_m$  is imposed on the dc bias current of a laser diode, a time variation of the diode frequency is produced and is described by:

$$\frac{d\phi}{dt} = \bar{\omega} + \beta \cos \omega_m t \quad (1)$$

$\beta$  is a frequency amplitude factor derived from the transformation of the sinusoidal current amplitude to frequency, and  $\bar{\omega}$  is the mean frequency of the diode laser determined by the case temperature, dc bias current, and the individual characteristics of the laser diode.  $\beta$  is set by adjusting the sinusoidal current input amplitude and is typically on the order of 200 Hz.

The laser radiation can be described by:

$$E(\omega) = E_0 \cos \phi, \text{ where } \frac{d\phi}{dt} = \bar{\omega} + \beta \cos \omega_m t$$

$$\therefore \phi = \bar{\omega} t + \frac{\beta}{\omega_m} \sin \omega_m t, \text{ and}$$

$$E(\omega) = E_0 \cos \left( \bar{\omega} t + \frac{\beta}{\omega_m} \sin \omega_m t \right) \quad (2)$$

$$\begin{aligned} E(\omega) &= E_0 \cos \bar{\omega} t \left[ J_0 \left( \frac{\beta}{\omega_m} \right) + 2 \sum_{n=1}^{\infty} J_{2n} \left( \frac{\beta}{\omega_m} \right) \cos 2n \omega_m t \right] \\ &- E_0 \sin \bar{\omega} t \left[ 2 \sum_{n=0}^{\infty} J_{2n+1} \left( \frac{\beta}{\omega_m} \right) \sin (2n+1) \omega_m t \right] \quad (3) \end{aligned}$$

$$\begin{aligned} E(\omega) &= E_0 \left[ J_0 \left( \frac{\beta}{\omega_m} \right) \cos \bar{\omega} t + \sum_{n=1}^{\infty} J_{2n} \left( \frac{\beta}{\omega_m} \right) [\cos (\bar{\omega} + 2n \omega_m) t \right. \right. \\ &+ \cos (\bar{\omega} - 2n \omega_m) t] + \sum_{n=0}^{\infty} J_{2n+1} \left( \frac{\beta}{\omega_m} \right) [\cos (\bar{\omega} + (2n+1) \omega_m) t \\ &\left. \left. - \cos (\bar{\omega} - (2n+1) \omega_m) t] \right] \quad (4) \end{aligned}$$

where  $J_n(x)$  is the Bessel function of order  $n$ .

A graphical representation of the Fourier components of  $E(\omega)$  is shown in figure 1.

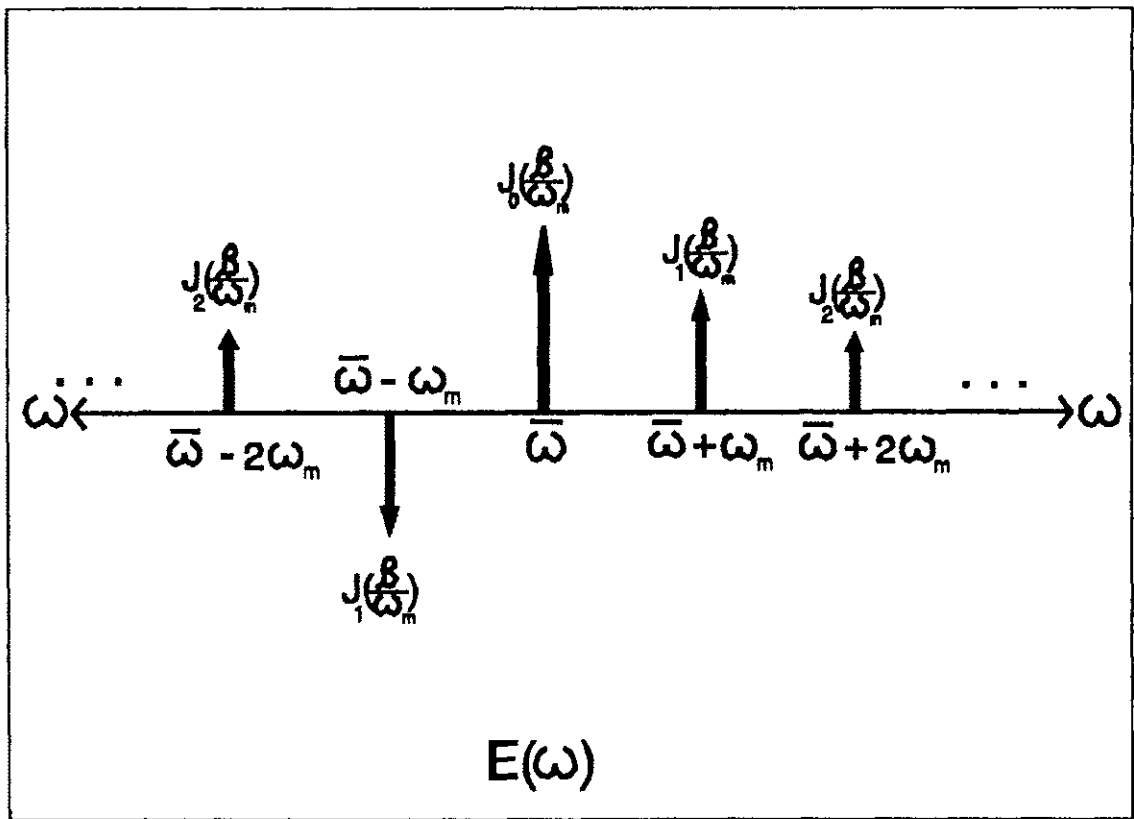


Figure 1 Fourier Components of a Modulated Diode Laser Beam.

## Frequency Modulation and Derivative Spectroscopy

The frequency modulated diode laser can be used to produce the derivatives of weak absorption profiles on a lock-in amplifier. Upon entering an absorbing medium and traveling a distance  $d$ , each Fourier component of the modulated laser beam will experience a decrease described by the Beer-Lambert law:

$$\bar{E}(\omega) = E(\omega) e^{-\alpha(\omega) \frac{d}{2}} e^{-i\theta(\omega) d} \Delta E(\omega) \gamma(\omega) e^{-i\theta(\omega) d} \quad (5)$$

where  $\alpha(\omega)$  is the absorption coefficient, which corresponds to the imaginary part of the index of refraction, and  $\Theta(\omega)$  contains phase information related to the real part.

The modulated laser beam can now be described by:

$$\begin{aligned} \bar{E}(\omega) = & E_0 \left[ J_0 \left( \frac{\beta}{\omega_m} \right) \gamma(\bar{\omega}) e^{-i\theta(\bar{\omega}) d} \cos \bar{\omega} t + \right. \\ & \sum_{n=1}^{\infty} J_{2n} \left( \frac{\beta}{\omega_m} \right) [\gamma(\bar{\omega} + 2n\omega_m) e^{-i\theta(\bar{\omega} + 2n\omega_m) d} \cos(\bar{\omega} + 2n\omega_m) t + \\ & \left. \gamma(\bar{\omega} - 2n\omega_m) e^{-i\theta(\bar{\omega} - 2n\omega_m) d} \cos(\bar{\omega} - 2n\omega_m) t] \right. \\ & + \sum_{n=0}^{\infty} J_{2n+1} \left( \frac{\beta}{\omega_m} \right) [\gamma(\bar{\omega} + (2n+1)\omega_m) e^{-i\theta(\bar{\omega} + (2n+1)\omega_m) d} \cos(\bar{\omega} + (2n+1)\omega_m) t \\ & \left. - \gamma(\bar{\omega} - (2n+1)\omega_m) e^{-i\theta(\bar{\omega} - (2n+1)\omega_m) d} \cos(\bar{\omega} - (2n+1)\omega_m) t] \right] \quad (6) \end{aligned}$$

This can be expressed in the simpler form:

$$\bar{E}(\omega) = E_0 \left[ \sum_{n=-\infty}^{\infty} \Phi(n) J_{|n|} \left( \frac{\beta}{\omega_m} \right) \gamma(\bar{\omega} + n\omega_m) e^{-i\theta(\bar{\omega} + n\omega_m)d} \cos(\bar{\omega} + n\omega_m)t \right] \quad (7)$$

$$\begin{aligned} \text{where } \Phi(n) &= -1 \text{ for } n = -1, -3, -5, \dots \\ &= 1 \text{ otherwise} \end{aligned}$$

After passing through the absorbing gas, the laser beam is measured on a photodiode. Since the detected signal is proportional to  $\bar{E}(\omega) \cdot \bar{E}^*(\omega)$ , the power incident on the detector is proportional to:

$$\begin{aligned} \bar{E}(\omega) \bar{E}^*(\omega) &= |E_0|^2 \left[ \sum_{n=-\infty}^{\infty} \Phi(n) J_{|n|} \left( \frac{\beta}{\omega_m} \right) \gamma(\bar{\omega} + n\omega_m) e^{-i\theta(\bar{\omega} + n\omega_m)d} \cos(\bar{\omega} + n\omega_m)t \right] \\ &\cdot \left[ \sum_{p=-\infty}^{\infty} \Phi(p) J_{|p|} \left( \frac{\beta}{\omega_m} \right) \gamma(\bar{\omega} + p\omega_m) e^{i\theta(\bar{\omega} + p\omega_m)d} \cos(\bar{\omega} + p\omega_m)t \right] \quad (8) \end{aligned}$$

$$\begin{aligned} \bar{E}(\omega) \bar{E}^*(\omega) &= |E_0|^2 \left[ \sum_{n=-\infty}^{\infty} \sum_{p=-\infty}^{\infty} \Phi(n) \Phi(p) J_{|n|} \left( \frac{\beta}{\omega_m} \right) J_{|p|} \left( \frac{\beta}{\omega_m} \right) \gamma(\bar{\omega} + n\omega_m) \cdot \right. \\ &\left. \gamma(\bar{\omega} + p\omega_m) e^{i[\theta(\bar{\omega} + p\omega_m) - \theta(\bar{\omega} + n\omega_m)]d} \cos(\bar{\omega} + n\omega_m)t \cos(\bar{\omega} + p\omega_m)t \right] \quad (9) \end{aligned}$$

For weak absorption and a small modulation index,

$$\gamma(\omega_1)\gamma(\omega_2) = e^{-[\alpha(\omega_1) + \alpha(\omega_2)] \frac{d}{2}} = 1 - \alpha(\omega_1) \frac{d}{2} - \alpha(\omega_2) \frac{d}{2}$$

$$\text{and for small } \left(\frac{\beta}{\omega_m}\right), \quad J_{|n|}\left(\frac{\beta}{\omega_m}\right) = \frac{\left(\frac{\beta}{\omega_m}\right)^{|n|}}{2^{|n|}|n|!} \quad [4] \quad (10)$$

$$J_{|n|}\left(\frac{\beta}{\omega_m}\right)J_{|p|}\left(\frac{\beta}{\omega_m}\right) = \frac{\left(\frac{\beta}{\omega_m}\right)^{|n|+|p|}}{|n|!|p|!2^{|n|+|p|}}$$

Also, for  $\omega_m \ll \Delta\omega$ ,  $\theta(\bar{\omega} + n\omega_m) = \theta(\bar{\omega} + p\omega_m)$ ,  $e^{i[\theta(\bar{\omega} + p\omega_m) - \theta(\bar{\omega} + n\omega_m)]} = 1$   
over several orders of  $|n-p|$

Therefore, the detector signal is proportional to:

$$\begin{aligned} \bar{E}(\omega)\bar{E}^*(\omega) = & |E_0|^2 \left[ \sum_{n=-\infty}^{\infty} \sum_{p=-\infty}^{\infty} \Phi(n)\Phi(p) \frac{\left(\frac{\beta}{\omega_m}\right)^{|n|+|p|}}{|n|!|p|!2^{|n|+|p|+1}} [1 - \alpha(\bar{\omega} + n\omega_m) \right. \\ & \left. - \alpha(\bar{\omega} + p\omega_m) \frac{d}{2}] [\cos(2\bar{\omega} + (n+p)\omega_m)t + \cos((n-p)\omega_m)t] \right] \quad (11) \end{aligned}$$

With an input reference frequency at  $\omega_m$ , the lock-in amplifier will process the detector signal by:

$$H \propto \frac{1}{T} \int_0^T \bar{E}(\omega) \bar{E}^*(\omega) \cos(h\omega_m) t dt \quad (12)$$

$$h \geq 1.$$

where H is the lock-in amplifier output, and h is an integer corresponding to the lock-in amplifier harmonic setting. The bandwidth of the lock-in amplifier used in this experiment was limited to  $0 < h\omega_m \leq 100$  KHz.

It can be seen that for all components of the detector signal with frequencies not equal to  $h\omega_m$ ,  $H = 0$ . The other components will contribute 1/2 their magnitudes.

From equations (11) and (12), the only contributing factors will satisfy the following equations:

$$h = |n - p|, \quad (13a) \quad \text{and} \quad h = \frac{2\bar{\omega}}{\omega_m} + n + p \quad (13b)$$

For  $h = \frac{2\bar{\omega}}{\omega_m} + n + p$ ,  $2\bar{\omega} \gg \omega_m$  and  $\therefore |n|$  or  $|p|$  becomes large.

$$\text{This causes } J_{|n|}\left(\frac{\beta}{\omega_m}\right) \cdot J_{|p|}\left(\frac{\beta}{\omega_m}\right) = 0.$$

Therefore, the only components that will appear in the lock-in amplifier output will be terms that satisfy (13a).

The lock-in amplifier output, H, will therefore be:

$$H \propto \sum_n \sum_p \Phi(n) \Phi(p) \frac{\left(\frac{\beta}{\omega_m}\right)^{|n|+|p|}}{|n|!|p|!2^{(|n|+|p|+2)}} \left(1 - \alpha(\bar{\omega} + n\omega_m) \frac{d}{2} - \alpha(\bar{\omega} + p\omega_m) \frac{d}{2}\right) \quad (14)$$

$$\text{for } h = |n - p|$$

It can be shown that H is proportional to the derivatives of the absorption profile. For  $h = 1$  and 2, H becomes:

$$H_{h=1} \propto |E_0|^2 \frac{\left(\frac{\beta}{\omega_m}\right) \cdot d}{4} \cdot \frac{(\alpha(\bar{\omega} - \omega_m) - \alpha(\bar{\omega} + \omega_m))}{2} = |E_0|^2 \frac{\left(\frac{\beta}{\omega_m}\right)}{4} \frac{d\alpha(\omega)}{d\omega} \Big|_{\omega=\bar{\omega}} \quad (15)$$

$$\text{for } \omega_m \ll \bar{\omega}, \Delta\omega$$

$$H_{h=2} \propto |E_0|^2 \frac{\left(\frac{\beta}{\omega_m}\right)^2 \cdot d}{2^3} \cdot \frac{(\alpha(\bar{\omega} + \omega_m) - 2\alpha(\bar{\omega}) + \alpha(\bar{\omega} - \omega_m))}{2^2} = |E_0|^2 \frac{\left(\frac{\beta}{\omega_m}\right)^2 \cdot d}{2^3} \frac{d^2\alpha(\omega)}{d\omega^2} \Big|_{\omega=\bar{\omega}} \quad (16)$$

$$\text{for } \omega_m \ll \bar{\omega}, \Delta\omega$$

By choosing different harmonics, several different derivatives can be selected.

A general form for lock-in amplifier processed signals is:

$$H_h(\bar{\omega}) \propto |E_0|^2 2^{-(h+1)} \cdot d \left( \frac{\beta}{\omega_m} \right)^h \frac{d^h \alpha(\omega)}{d\omega^h} \Big|_{\omega = \bar{\omega}} \quad (17)$$

*for*  $h \geq 1$ .

With the application of a low frequency ramp to the dc bias current, the mean frequency,  $\bar{\omega}$ , is tuned over the absorption profile, and an entire derivative for the profile is produced. This treatment is in good agreement with J. Reid and D. Labrie, 1981 [1].

From equation (17), it can be seen that the lock-in amplifier signal is dependent on the normalized modulation index,  $\beta/\omega_m$ . In the formulation of the general expression of equation (17), it was assumed that the normalized modulation index is small. Although the strength of the signal depends on the modulation index, the latter cannot be made comparable to one, since then the signal obtained will deviate from the derivative of the lineshape profile. In this work, the normalized modulation index was kept small enough to ensure that the condition given by equation (10) was satisfied.

### **Lineshape Functions**

The lineshape function of a transition is extremely important when determining the frequency characteristics of an absorption profile. In general, the absorption

profile,  $\alpha(\omega)$ , is proportional to  $n\sigma(\omega)$ , where  $n$  is the concentration of the absorbing molecules, and  $\sigma(\omega)$  is the absorption cross-section. In general, the lineshape function determines the frequency response of  $\sigma(\omega)$  [2]:

$$\sigma(\omega) = \bar{\sigma} \cdot g(\omega) \quad (18)$$

$\bar{\sigma}$  is defined as the integrated cross-section and  $g(\omega)$  is the lineshape profile for the transition. This integrated absorption cross-section can be derived from [2]:

$$\begin{aligned} \sigma(\omega) &= \bar{\sigma} g(\omega), \quad \int_0^{\infty} \sigma(\omega) d\omega = \bar{\sigma} \int_0^{\infty} g(\omega) d\omega \\ \therefore \bar{\sigma} &= \frac{1}{2\pi} \int_0^{\infty} \sigma(\omega) d\omega \text{ in units of } \text{cm}^2 \text{ s}^{-1} \end{aligned} \quad (19)$$

Lineshape functions are usually characterized into the categories of inhomogeneous broadened, homogeneous broadened or some combination of inhomogeneous and homogeneous broadened.

### Gaussian Profiles

The term *inhomogeneous* means that individual atoms/molecules within a collection of otherwise identical atoms/molecules do not have the same resonant response frequencies [2]. Therefore, in an inhomogeneously broadened profile, each

atom/molecule contributes unevenly to the strength of the line in a given frequency interval.

A common example of inhomogeneous broadening is due to the Doppler effect. This profile can be described by a Gaussian lineshape given by [2]:

$$g_G(\omega) = \frac{2\pi}{\delta\omega_G} \left( \frac{4 \ln 2}{\pi} \right)^{1/2} e^{-\frac{4(\omega - \omega_0)^2 \ln 2}{\delta\omega_G^2}}, \quad \delta\omega_G = 2 \frac{\omega_0}{c} \left( 2 \frac{kT}{M_x} \ln 2 \right)^{1/2} \quad (20)$$

$\delta\omega_G$  is the FWHM for the line.

The dominant inhomogeneous broadening mechanism for the Oxygen A-band transitions in this research is Doppler broadening. For low pressures, the Doppler broadened Gaussian lineshape function is the dominant profile and  $g(\omega)$  can be approximated by  $g_G(\omega)$ .

### Lorentzian Profiles

*Homogeneously* broadened lineshape functions are described by broadening mechanisms that affect all of the individual atoms in a collection in exactly the same way.

In general, homogenous broadened lineshape functions are described by a Lorentzian lineshape given by [2]:

$$g_L(\omega) = \frac{\Delta\omega_L}{(\omega_0 - \omega)^2 + (\Delta\omega_L/2)^2} \quad (21)$$

The dominant homogeneous broadening mechanism for the Oxygen A-band transitions in this research is collision broadening which causes a dephasing of the wave functions of the Oxygen molecules upon collision. For such molecules, the collision-broadened Lorentzian lineshape becomes dominant at roughly 1/2 atmosphere of air. Because there are more collisions at higher concentrations of gas molecules, the full width at half maximum (FWHM) is generally a function of pressure.

An expression for the collisional Lorentzian FWHM is given by [2]:

$$\begin{aligned} \Delta\omega_L \approx & \Delta\omega_n + \Delta\omega_I + 2\pi n_{O_2} \sigma_{coll_{O_2}} \left[ \frac{8kT}{\pi} \left( \frac{2}{M_{O_2}} \right) \right]^{1/2} \\ & + 2\pi n_{N_2} \sigma_{coll_{N_2}} \left[ \frac{8kT}{\pi} \left( \frac{1}{M_{O_2}} + \frac{1}{M_{N_2}} \right) \right]^{1/2} \end{aligned} \quad (22)$$

where  $\Delta\omega_n$  is the natural linewidth, and  $\Delta\omega_I$  is an empirical residual linewidth that expresses the fact that the collision linewidth increases with pressure from an initial value approximately equal to the Doppler linewidth. The expected value of  $\Delta\omega_I$  is on the order of  $2\pi \cdot 10^9$  rad/s, which is a typical Doppler FWHM. This mathematical treatment is in good agreement with our experimental data from which we found that  $\Delta\omega_I \approx 4.6 \cdot 10^9$  rad/s (see Chapter III).

For the A-band transitions utilized, natural broadening was on the order of 1 Hz [5]. Compared to a minimal Doppler broadening of GHz, a natural line width on the order of 1 Hz is insignificant, and was therefore not included in any calculations.

### Voight Profile

Neither the Gaussian Doppler, nor the Lorentzian collisional lineshape functions give a precise match over all values of gas concentration. A more accurate representation over all values of gas concentration is the Voight lineshape function, which is a convolution of the Doppler broadened lineshape function and the collisional broadened Lorentzian lineshape function. It can be thought of as a representation of the Lorentzian lineshape function with a Doppler shift caused by a velocity, integrated over a velocity distribution.

The general expression for the Voight lineshape function is [2]:

$$g_v(\omega) = \left(\frac{M_{O_2}}{2\pi kT}\right)^{1/2} \int_{-\infty}^{\infty} \left[ \frac{\Delta\omega}{\left(\omega_0 - \omega + \omega_0 \frac{v_z}{c}\right)^2 + \left(\frac{\Delta\omega}{2}\right)^2} \right] \exp\left(\frac{-M_{O_2} v_z^2}{2kT}\right) dv_z \quad (23)$$

Although the Voight function provides a complete solution, the integral in the Voight lineshape function cannot be solved in a closed form; tabulated values, however, are available. This makes working with the Voight function more difficult than the easily graphed Lorentzian and Gaussian lineshape functions. Since a closed form for the Voight profile does not exist, the analysis of derivatives of the Voight lineshape function is somewhat difficult.

### Our Approximation to the Voight Profile

It is clear that as the concentration of the absorbing gas molecules,  $n$ , approaches 0, the Voight function approaches a Gaussian lineshape profile. Similarly, as  $n$  is increased, the Voight profile approaches a Lorentzian lineshape profile. In order to approximate the Voight function, we formed a linear combination which satisfies these conditions; we call this combination the Voight lineshape approximation,  $g_{VA}(\omega)$ . The Voight lineshape approximation is easy to work with and provides excellent agreement with experimental results as is shown in Chapter III. The Voight approximation is a gas concentration weighted combination of a Gaussian lineshape function and a Lorentzian lineshape function. From this strategy and from trial and error, we found, for this experiment, that a good approximation for the Voight lineshape function is:

$$g_V(\omega) = g_{VA}(\omega) = C_G \cdot g_G(\omega) + C_L \cdot g_L(\omega) \quad (24)$$
$$\text{where } C_L = \frac{n^2}{n^2 + n_{\delta,2}^2} \text{ and } C_G = 1 - C_L = \frac{n_{\delta,2}^2}{n^2 + n_{\delta,2}^2}$$

The value of  $n_{\delta,2}$  is interpreted as the gas concentration turning point that gives the density at which the Doppler and collision mechanisms have equal weight.  $n_{\delta,2}$  can be said to define when the Voight lineshape function turns from the approximate Gaussian lineshape function to the approximate Lorentzian lineshape function. From this approach,  $C_L(n_{\delta,2}) = C_G(n_{\delta,2})$ . The value of  $n_{\delta,2}$  is gas specie and transition dependent. Excellent agreement with experimental results can be seen in Chapter III.

## Lineshape Derivatives

Since the output signal from the lock-in amplifier is proportional to the derivative of  $\alpha(\omega)$  with respect to  $\omega$ , the lineshape function derivatives for the transition under probe will appear in this signal. This can be seen by:

$$\frac{d^N \alpha(\omega)}{d\omega^N} = \frac{d^N [n\sigma(\omega)]}{d\omega^N} = \frac{n\bar{\sigma} d^N g(\omega)}{d\omega^N} = n\bar{\sigma} g^N(\omega) \quad (25)$$

With the development of derivative spectroscopy it is necessary to develop the general expressions for the derivatives of the lineshape functions. A good understanding of at least the first few derivatives is needed to appreciate the information that can be extracted.

The expressions for  $g_L^N(\omega)$  and  $g_G^N(\omega)$  for  $N = 1, 2,$  and  $3$  are:

$$g_L^1(\omega) = (2\pi)^2 \frac{-\Delta\omega(\omega - \omega_0)}{\pi [(\omega - \omega_0)^2 + (\frac{\Delta\omega}{2})^2]^2} \quad (26a)$$

$$g_L^2(\omega) = (2\pi)^3 \frac{\Delta\omega}{\pi} \cdot \frac{[3(\omega - \omega_0)^2 - (\frac{\Delta\omega}{2})^2]}{[(\omega - \omega_0)^2 + (\frac{\Delta\omega}{2})^2]^3} \quad (26b)$$

$$g_L^3 = (2\pi)^4 \frac{\Delta\omega}{\pi} \cdot \frac{-[12(\omega - \omega_0)^3 - 12(\omega - \omega_0)(\frac{\Delta\omega}{2})^2]}{[(\omega - \omega_0)^2 + (\frac{\Delta\omega}{2})^2]^4} \quad (26c)$$

$$g_G^1(\omega) = (2\pi)^2 \frac{-2(\omega - \omega_0)}{\sqrt{\pi} \Delta\omega_G^3} e^{-\frac{(\omega - \omega_0)^2}{\Delta\omega_G^2}} \quad (27a)$$

$$g_G^2(\omega) = (2\pi)^3 \frac{2}{\sqrt{\pi} \cdot \Delta\omega_G^5} \{2(\omega - \omega_0)^2 - 1\} e^{-\frac{(\omega - \omega_0)^2}{\Delta\omega_G^2}} \quad (27b)$$

$$g_G^3(\omega) = (2\pi)^4 \frac{4(\omega - \omega_0)}{\sqrt{\pi} \Delta\omega_G^5} \left\{3 - \frac{2(\omega - \omega_0)^2}{\Delta\omega_G^2}\right\} e^{-\frac{(\omega - \omega_0)^2}{\Delta\omega_G^2}} \quad (27c)$$

$$\text{where } \Delta\omega_G = \frac{\delta\omega_G}{\sqrt{4\ln 2}}$$

The graphs for the Gaussian and Lorentzian functions and their respective first and second derivatives are shown in figures 2 and 3 with the pertinent details labeled. For convenience, the lineshapes are shown in units of frequency.

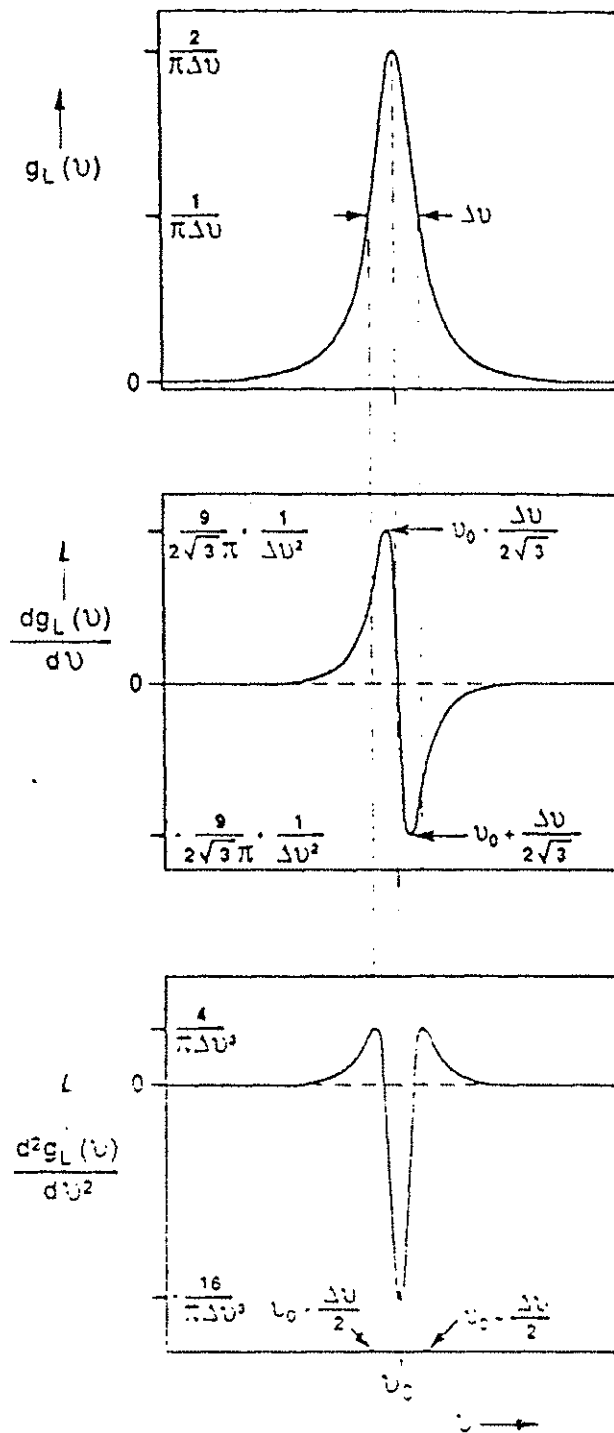


**Figure 2 Lorentzian Lineshape and Derivatives**

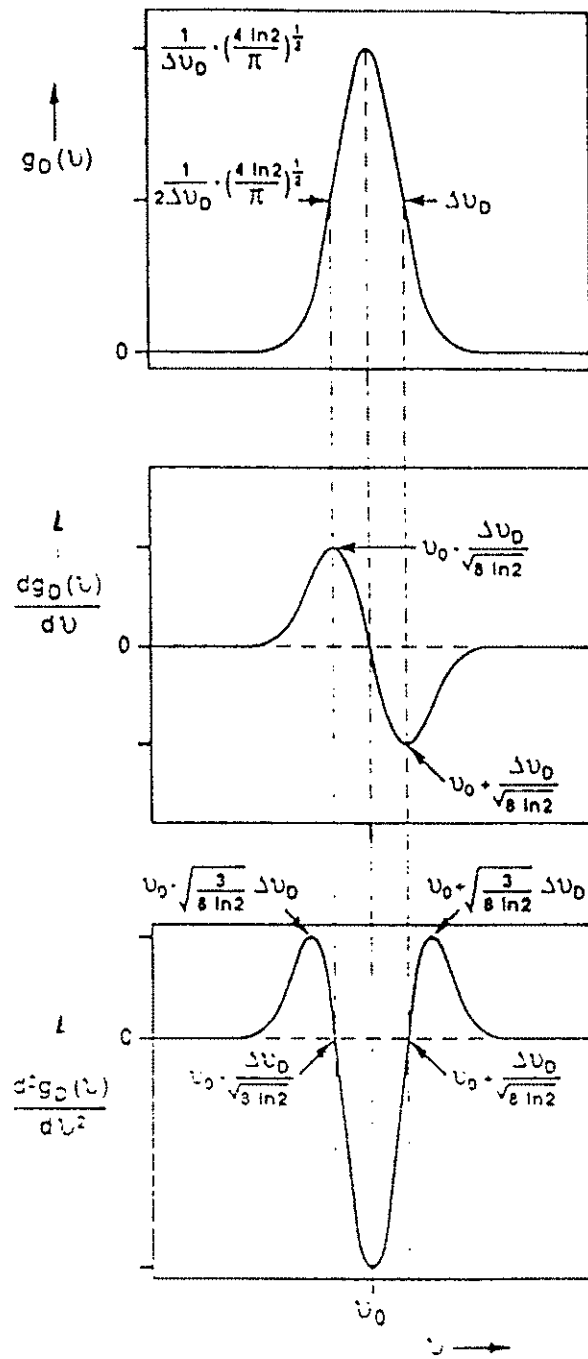


Figure 3 Gaussian Lineshape and Derivatives

Information from the derivatives can easily be extracted from the turning points of the corresponding plots.

In the limit that a lineshape approaches a Gaussian or a Lorentzian function, gas concentration or gas temperature can be obtained in a straight forward manner. The collisional-Lorentzian FWHM is a function of gas concentration and therefore the latter can be extracted from it. Similarly, the Doppler FWHM is a function of temperature, and therefore gas temperature can be obtained also.

Also, a detailed examination of the absorption profile further and further into the wings (away from linecenter) is possible with the use of higher order derivative spectroscopy, and the examination of lineshape distortions not normally associated with Gaussian or Lorentzian lineshape functions can be closely examined. Another possible use of higher order derivative spectroscopy is in the separation of two or more frequency close absorption lines. With higher derivatives, the features of each absorption line may possibly be extracted.

Although more detailed information can be extracted with higher derivatives, it can from equation (17) that there is a tradeoff between higher derivatives and signal strength. This must be taken into consideration, especially with weaker lines.

For derivative absorption spectroscopy, the Nth order derivative for a lineshape is needed to make any theoretical calculations and to extract information from an Nth order derivative absorption signal. These derivatives may be computed, but this may be quite time consuming for higher order derivatives. For convenience, general expressions have been developed for the Nth order derivative of the Gaussian and the

Nth order derivative of the Lorentzian lineshape functions. These general expressions have been mathematically proven by induction[3] and have been shown to be:

$$g_L^N(\omega) = (2\pi)^N (\Delta\omega) \frac{(-1)^N}{y^{N+1}} \sum_{k=0}^{\lfloor N/2 \rfloor} C_{2k,N} \left(\frac{\Delta\omega}{2}\right)^{2k} (\omega - \omega_0)^{N-2k}, \quad (28)$$

$$y = (\omega - \omega_0)^2 + \left(\frac{\Delta\omega}{2}\right)^2$$

where  $[N] = N - 1$  if  $N$  is odd  $[N] = N$  if  $N$  is even

$$C_{2k,N} = (-1)^k \frac{(N+1)!}{2k+1} \binom{N}{2k}, \text{ and } \binom{N}{2k} = \frac{N!}{(2k)! (N-2k)!}$$

$$g_G^N(\omega) = \frac{g}{\sqrt{\pi}} \frac{(2\pi)^{N+1}}{(\Delta\omega_D)^{2N+1}} \sum_{k=0}^{\lfloor N/2 \rfloor} C_{2k,N} (\Delta\omega_D)^{2k} (\omega - \omega_0)^{N-2k} \quad (29)$$

where  $g = \exp\left[\frac{-(\omega - \omega_0)^2}{(\Delta\omega_D)^2}\right]$ ,

$$C_{2k,N} = (-1)^k \frac{N!}{(N-2k)!} \frac{(-2)^{N-2k}}{k!} \text{ and } \begin{cases} [N] = N-1 & \text{for } N \text{ odd} \\ [N] = N & \text{for } N \text{ even} \end{cases}$$

Since the Voigt function is difficult to work with, a general second derivative approximation for the Voigt lineshape function was formed by:

$$g^2_{VA}(\omega) = C_G \cdot g^2_G(\omega) + C_L \cdot g^2_L(\omega)$$

$$\text{where } C_L = \frac{n^2}{n^2 + n_{b,2}^2} \text{ and } C_G = 1 - C_L = \frac{n_{b,2}^2}{n^2 + n_{b,2}^2} \quad (30)$$

### Measurement of Concentration and Temperature

Gas concentration measurements may be taken from the direct absorption signal and/or any of its derivatives. For this thesis, the information was taken from the second derivative of the absorption lineshape. The second derivative signal was chosen because one need not go up to any higher order derivatives, since the effects of the ramp sweep are eliminated for the second and higher derivatives. Furthermore, it was convenient and exhibited a strong peak that corresponded to linecenter. The gas examined was Oxygen, and the transitions examined were in the Oxygen A-band (See Figure 4 below).

#### Concentration

In general, the second harmonic signal obtained on the lock-in amplifier will be proportional to:

$$E_o^2 n \bar{\sigma} d \cdot \frac{d^2 g(\omega)}{d\omega^2} \quad (31)$$

where  $n$  is the oxygen concentration,  $\bar{\sigma}$  is the integrated cross-section for the absorption line probed,  $d$  is the length of the chamber, and  $g(\omega)$  is the lineshape function.

The second derivative of the lineshape function at line center is given by:

$$\text{For the Gaussian: } \frac{d^2 g_G(\omega)}{d\omega^2} \Big|_{\omega=\omega_0} = \frac{-4(2\pi)^3 \sqrt{\ln(2)}}{\sqrt{\pi} \Delta \omega_G^3} \quad (32)$$

$$\text{For the Lorentzian: } \frac{d^2 g_L(\omega)}{d\omega^2} \Big|_{\omega=\omega_0} = \frac{-32 \cdot (2\pi)^2}{\Delta \omega_L^3} \quad (33)$$

In the low-pressure Doppler regime, the lineshape function can be considered purely Gaussian. For this case, the lock-in amplifier signal at line center is a linear function of oxygen concentration given by:

$$S_G \propto n \cdot \frac{|E_0|^2 \left( \frac{\beta}{\omega_m} \right)^2 \bar{\sigma} d (2\pi)^3 \sqrt{\ln(2)}}{2 \Delta \omega_D^3} \quad (34)$$

This is in excellent agreement with our experimental results (see Chapter III).

In the higher-pressure collision broadened regime, the lineshape function can be considered purely Lorentzian. The lock-in amplifier signal at line center for this case is given by:

$$S_L \propto n \cdot \frac{4(2\pi)^2 |E_0|^2 \left(\frac{\beta}{\omega_m}\right)^2 \bar{\sigma} d}{\Delta \omega_L^3} \quad (35)$$

For this case, the lock-in amplifier signal at line center will show a  $1/n^2$  dependence, since the collisional FWHM is itself a function of  $n$  (see equation 22). Hence, one expects a linear dependence on  $n$  (the Doppler regime) gradually turning to a  $1/n^2$  dependence (the collisional regime). Experimental results discussed in Chapter III are in excellent agreement with this prediction.

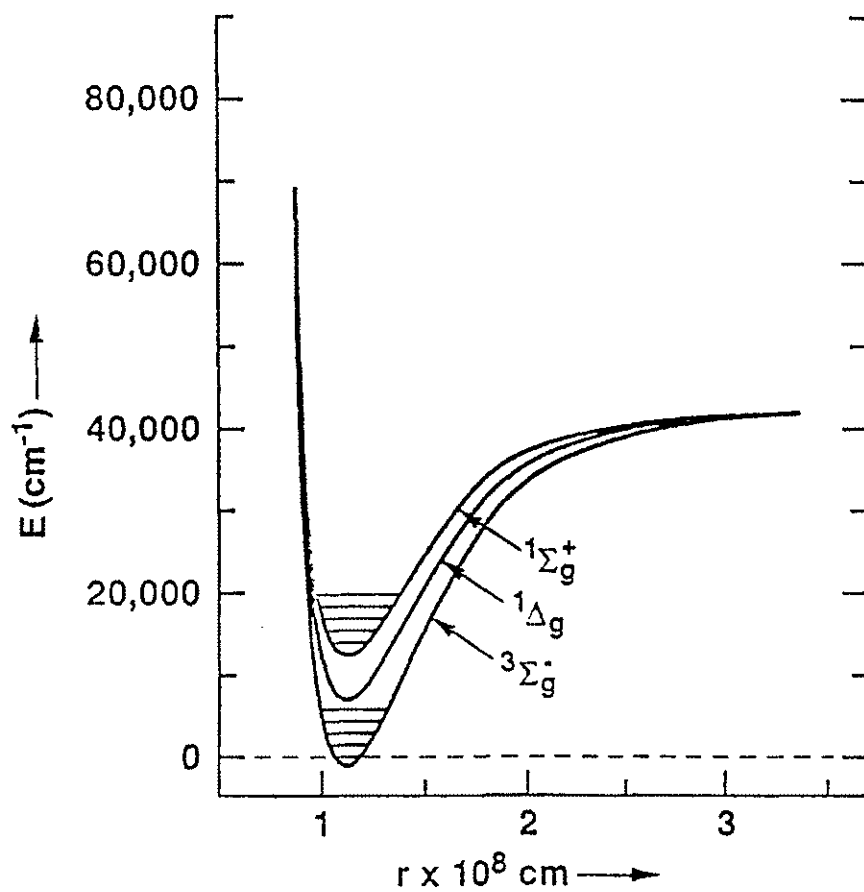
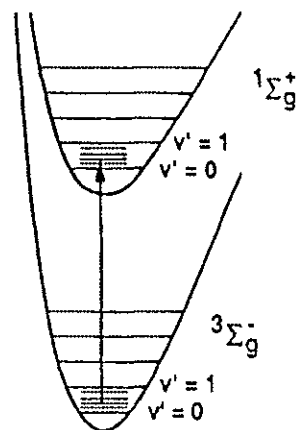
### Temperature

The measurement of temperature may be accomplished by simultaneously examining the strengths of two different rovibronic spectral lines. In the case of the measurements made here, all transitions examined are in the Oxygen A-band. This means that all transitions originate from the zeroth vibrational quantum in the ground electronic state, and they end in zeroth vibrational quantum in the excited state

( $b \ ^1\Sigma_g^+ \leftarrow X \ ^3\Sigma_g^-$ ;  $v''=0, v'=0$ ). Figure 4 shows the general potential energy curves

for oxygen with an inset for the Oxygen A-band.

O<sub>2</sub> A BAND TRANSITIONS



LOWER ELECTRONIC STATES OF O<sub>2</sub>

In this research, the lock-in amplifier second derivative signal at line center was examined for temperature information. From equation 31, the general expressions for the second derivative signal at line center for two different rovibronic lines are:

$$S(\omega_{01}) = |E_0|^2 n_1 \bar{\sigma}_1 d \frac{d^2 g_1(\omega)}{d\omega^2} \Big|_{\omega = \omega_{01}}$$

$$S(\omega_{02}) = |E_0|^2 n_2 \bar{\sigma}_2 d \frac{d^2 g_2(\omega)}{d\omega^2} \Big|_{\omega = \omega_{02}}$$

The ratio of the two lines is given by:

$$R \equiv \frac{S(\omega_{01})}{S(\omega_{02})} = \frac{n_1 \bar{\sigma}_1 g''_1(\omega_{01})}{n_2 \bar{\sigma}_2 g''_2(\omega_{02})} \quad (36)$$

The thermal population density for the rotational levels is not simply given by the Boltzmann factor  $e^{-E/kT}$ ; we have to allow for the fact that, according to quantum theory, each state of an molecular system with total angular momentum  $J$  consists of  $2J+1$  levels; that is, the state has  $(2J+1)$ -fold degeneracy [6]. The frequency of occurrence (its statistical weight) is therefore  $(2J+1)$  times that of a state with  $J=0$ .

For most practical cases, a rigid rotator model can be used to determine the population distribution function; hence, the population distribution for a rotational level  $J$  is given by:

$$n \propto (2J+1) e^{-E_J/kT} \quad (37)$$

Taking the ratio of  $n_1/n_2$  yields:

$$\frac{n_1}{n_2} = \frac{(2J_1 + 1)}{(2J_2 + 1)} \cdot \exp(\Delta E/kT) \quad (38)$$

$$\text{where } \Delta E = \hbar(\omega_{02} - \omega_{01})$$

Hence, R becomes:

$$R \equiv \frac{S(\omega_{01})}{S(\omega_{02})} = \frac{(2J_1 + 1) \bar{\sigma}_1 g''_1(\omega_{01})}{(2J_2 + 1) \bar{\sigma}_2 g''_2(\omega_{02})} \cdot \exp(\Delta E/kT) \quad (39)$$

The integrated cross-section for each measured transition can be obtained from the HITRAN data tables available through NOAA on magnetic tape [14]. Also, from equations (32) and (33), it can easily be seen that:

$$\frac{g''_1(\omega_{01})}{g''_2(\omega_{02})} = \left( \frac{\Delta \omega_2}{\Delta \omega_1} \right)^3 \quad (40)$$

This is true for both the Gaussian and the Lorentzian lineshapes.

Solving the ratio expression for T yields:

$$T = \frac{\Delta E/k}{\ln \left( R \left( \frac{2J_2 + 1}{2J_1 + 1} \right) \frac{\bar{\sigma}_2 \left( \frac{\Delta \omega_1}{\Delta \omega_2} \right)^3}{\bar{\sigma}_1} \right)}, \quad (41)$$

from which it is seen that there is a strong reliance on the FWHM ratio of the lines.

The cubed dependence makes the temperature measurements very sensitive to changes (or measurement error) in the FWHM ratio. In the Doppler-broadened Gaussian

regime, this ratio is a constant independent of Oxygen concentration, but in the collision-broadened Lorentzian regime, the FWHM is concentration dependent. Careful measurement of the FWHM for each line is therefore needed to ensure accuracy in the measurement of temperature.

## **Chapter III.**

### **EXPERIMENTAL PROCEDURE AND RESULTS**

The basic experimental procedure used in the research for this thesis involved the current modulation of a diode laser by imposing a small sinusoidal current on the DC bias current of the diode and then probing various Oxygen A-band transitions in a sample of air at various pressures. To select an individual A-band transition, a rough frequency tuning is achieved by adjusting the case temperature of the diode laser with the temperature controller, and a fine tuning is achieved by adjusting the DC bias of the diode laser with the current controller. After passing through the sample cell, the modulated laser beam was measured on a photodiode, and the signal was processed with a lock-in amplifier. The second derivative signal of the absorption profile was used to extract concentration information, and by changing the reference harmonic of the lock-in amplifier, higher order derivatives were obtained.

#### **Experimental Arrangement**

The experimental arrangement used in this research is shown in figure 5. A Mitsubishi ML4405 diode laser installed in an ILX Lightwave LDM-4412 diode laser mount with an attached collimating lens was used. An ILX Lightwave LDT-5910B temperature controller provided course wavelength tuning, while an ILX Lightwave LDX-3620 ultra low noise current source was used to provide the DC bias current and

the current ramp. The slow current ramp provided the means to sweep the laser center frequency over the entire absorption frequency profile. The LDX-3620 was modified so that an external signal could be added with the ramp and DC bias; it was modified by ILX Lightwave at our request. An Exact 7030 signal generator with variable amplitude control was used to provide the small ac component of the laser diode current, which in turn provided the needed frequency modulation described in Chapter II. A Burleigh wavemeter was used to provide a frequency reference for the experiment. This wavemeter uses a Michelson interferometer and an internal reference HeNe laser to measure laser wavelength. An EG&G VT100 photodiode detector was used in the photovoltaic mode, and it was connected to the lock-in amplifier in a differential voltage connection configuration for lower noise pick-up; the basic configuration is given in reference [13]. A Stanford Research SR850 DSP lock-in amplifier was used for the phase sensitive detection. This lock-in amplifier multiplies the digitized signal with a digitally computed reference sine wave thus eliminating harmonic rejection problems that are associated with many lock-in amplifiers that use a square wave. A 1 meter long windowed chamber fitted with O-rings and Swagelok vacuum fittings was used to in conjunction with a mechanical Edwards roughing pump to maintain a number of air pressures and, therefore, Oxygen concentrations. A MKS Instruments PDR-D-1 digital pressure meter provided continuous monitoring of the chamber pressure with an accuracy within 0.4 Torr. This meter was calibrated to atmospheric pressure at the beginning of every test day. A Melles Griot 50-50 beam

splitter, two-inch diameter lenses for the near I, and flat mirrors were used for beam splitting, steering, collimating and focussing.

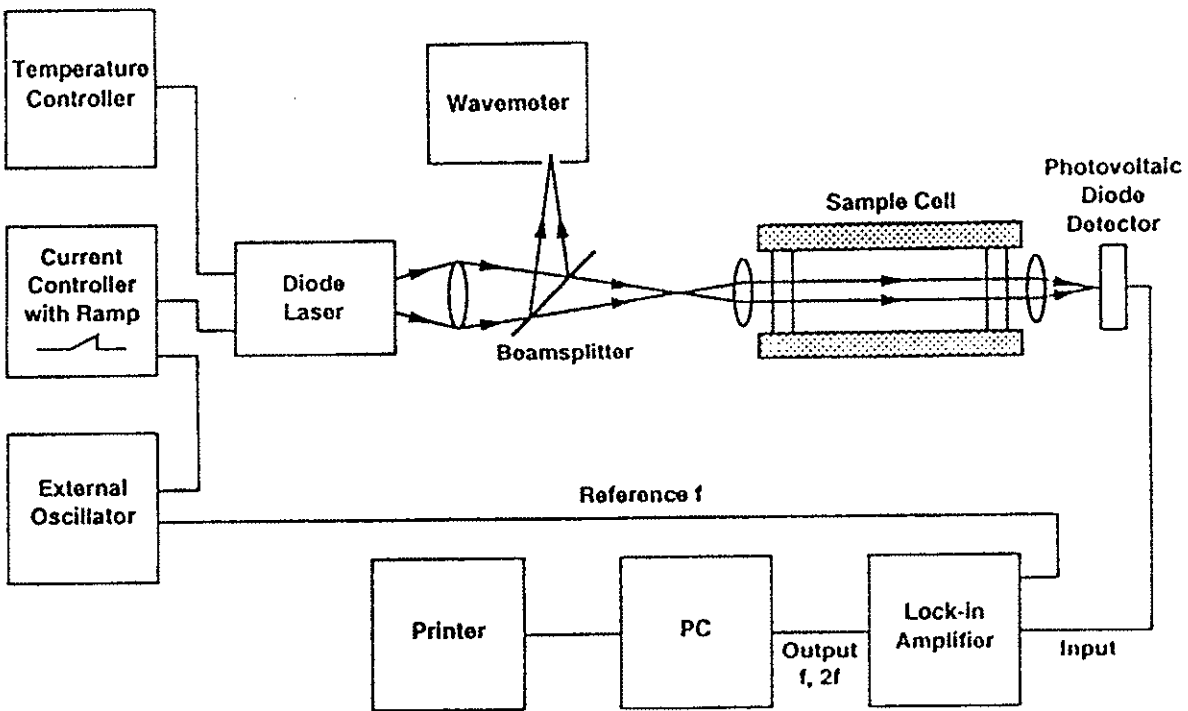


Figure 5 Experimental Apparatus

## **RQ(11,12) Line Measurements**

### Linewidth Measurements

The FWHM was obtained from the second derivative signal over several values of pressure. A total of 30 FWHM pressure measurements were taken. Each measurement was taken eight times, averaged, and plotted in figure 6. The measured FWHM was compared to the theoretical values for the Doppler-broadened FWHM and the collision-broadened FWHM (expressions in Chapter II). The results are shown in figure 6. Excellent agreement with the theoretical models was obtained.

In the low pressure Doppler broadened regime, it can be seen that the FWHM actually decreases by a small amount. It is believed that this is due to Dickie narrowing [5]. The line narrows by  $\approx 2\%$  of the total Doppler-broadened FWHM. In this type of line narrowing the Doppler component of the line profile is reduced in width due to collisions which restrict the translational freedom of the absorbing molecules [5]. This has also been seen in direct absorption measurements of the Oxygen A-band performed by Ritter and Wilkerson [5]. At about 80 torr, they found that Dickie narrowing was on the order of 4 % of the total Doppler-broadened FWHM for the RR(11,11) line. Hence, our measured value of 2% is very reasonable for the RQ(11,12) line.

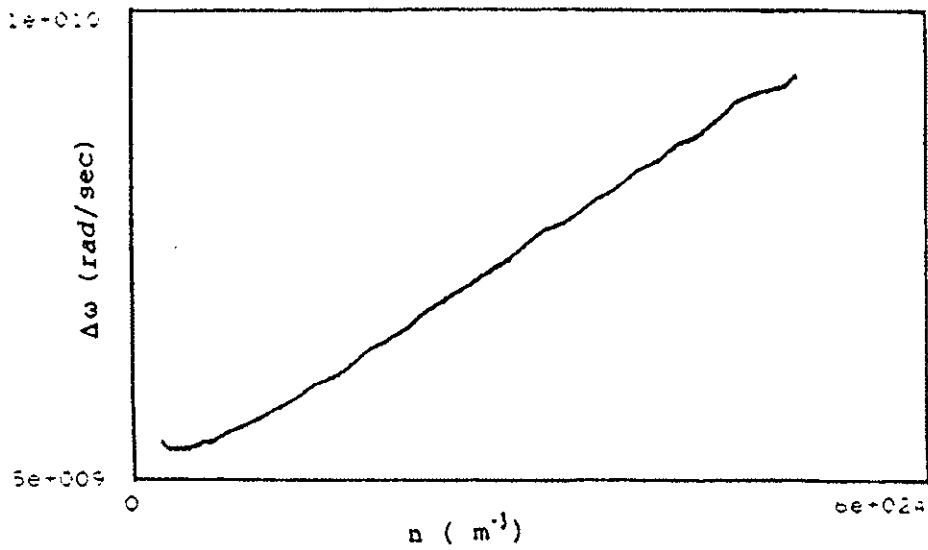


Figure 6(a) Measured FWHM vs. Oxygen Concentration

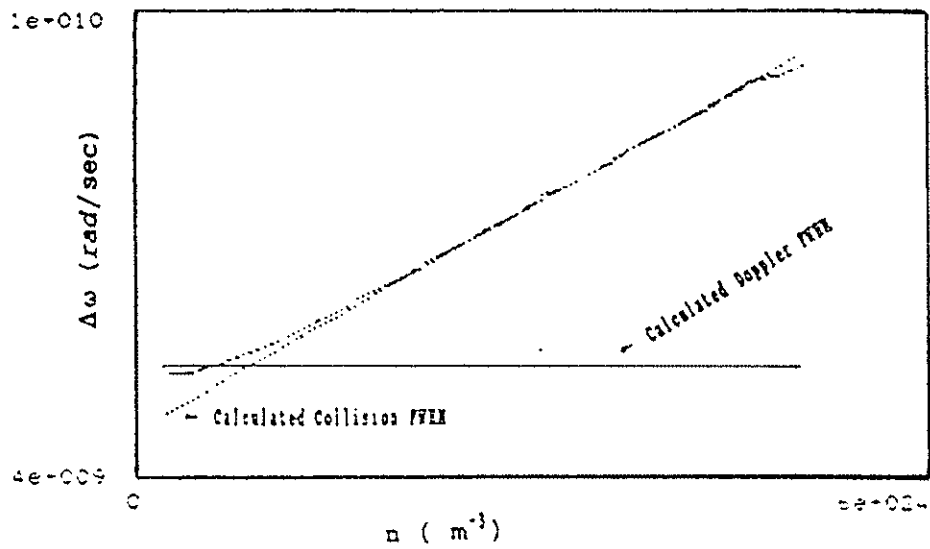


Figure 6(b) Measured and Calculated FWHM vs. Concentration

From the data obtained in figure 6(a) a value of the collisional cross-section can be obtained. By assuming the collisional cross-section for Oxygen with Oxygen and Oxygen with Nitrogen are approximately the same, and by knowing the fact that the density of Nitrogen is approximately 3.71 n, where n is the concentration of Oxygen in air, a collisional cross-section for Oxygen with air can be obtained by differentiating the expression in equation (22). (The assumption that collisional cross sections for Oxygen with Oxygen and Oxygen with Nitrogen are approximately the same is reasonable in light of the fact that the hard sphere molecular sizes are very nearly the same [6].

$$\frac{d\Delta\omega_L}{dn} = \sigma \cdot (2\pi) \left( \left[ \frac{8kT}{\pi} \left( \frac{2}{M_{O_2}} \right) \right]^{1/2} + 3.71 \left[ \frac{8kT}{\pi} \left( \frac{1}{M_{O_2}} + \frac{1}{M_{N_2}} \right) \right]^{1/2} \right) \quad (42)$$

From the slope of the FWHM in the collisional regime, a collisional cross-section of Oxygen with air was found to be  $\approx 1.59 \times 10^{-15} \text{ cm}^2$ . This cross-section was used in the theoretical plot of the collision-broadened FWHM shown in figure 6(b).

### Signal Magnitude

RQ(11,12) second derivative measurements were obtained for various air pressures. Figure 7 shows the second derivative signal measured at line center (760.445 nm) for 30 different concentrations. Each experimental point represents the average of 8 measurements. The maximum deviation from the average value was found to be  $\approx 4\%$ . The majority of the measurements were within 2% of the averaged value. Similar results were obtained for the FWHM measurements.

In the low pressure regime, a linear relationship with oxygen concentration is seen as expected. Here, collisional broadening is small compared to the Doppler broadening, and this gives the line a Doppler-broadened Gaussian behavior. As the pressure is increased, the collision-broadened FWHM becomes large in comparison to the Doppler FWHM, and the lineshape will take on the characteristics of a collision-broadened Lorentzian lineshape. This can be seen at higher pressures in the expected  $1/n^2$  signal relationship.

A calculated Doppler-broadened second derivative signal at line center and a calculated collision-broadened signal at line center are shown in figure 7(a). Excellent agreement between the experimental data and the calculated signals can be seen in their corresponding pressure regimes.

Figure 7(b) shows a theoretical model based on the approximation to the Voigt lineshape given by equation (30). An almost perfect match can be seen between the data and this mathematical model.

Dickie narrowing is small enough in comparison to the Doppler-broadened FWHM that it does not seem to appreciably affect the second derivative signal at line center.

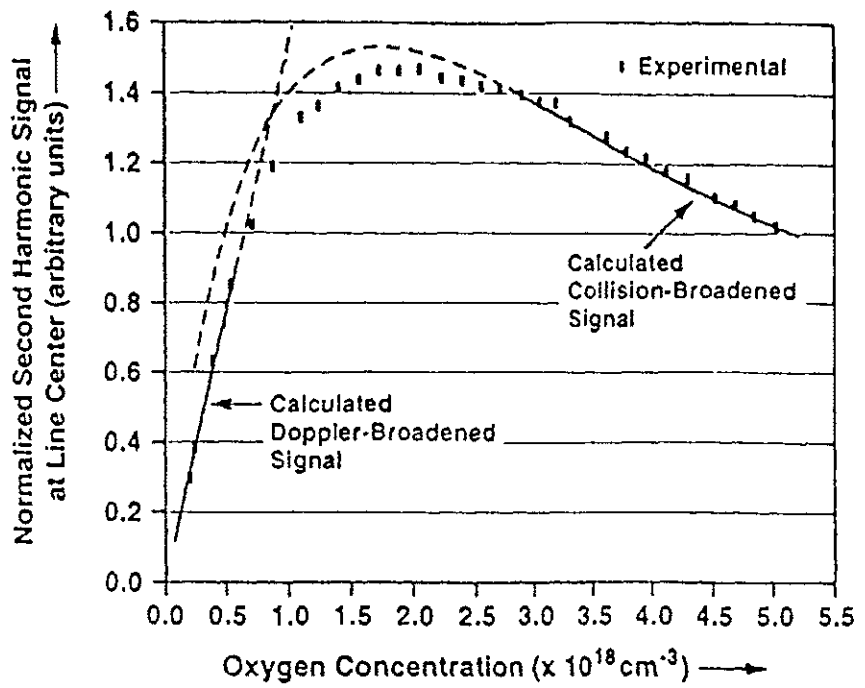


Figure 7(a) Second Harmonic Signal vs. Concentration With Calculated Broadening

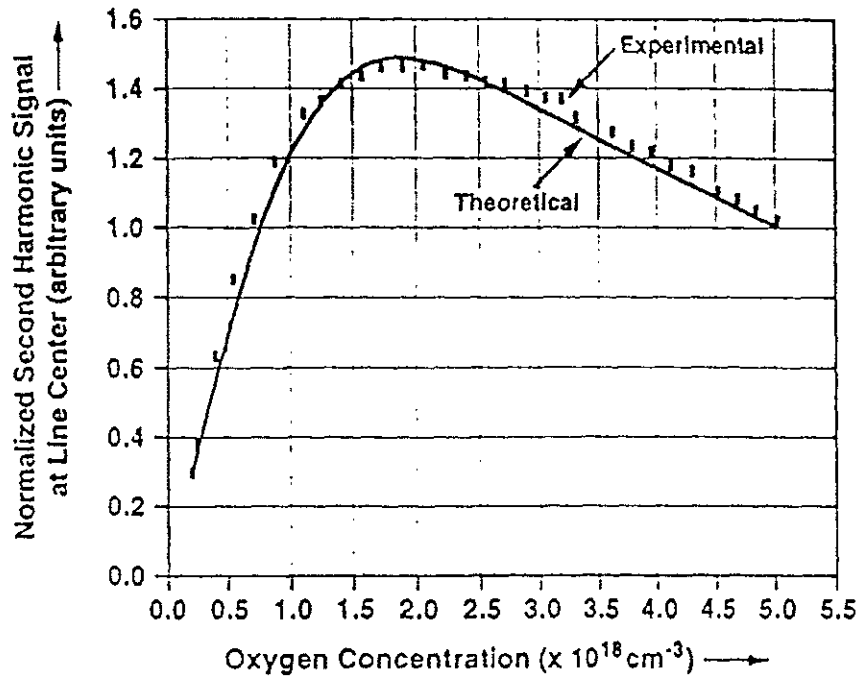


Figure 7(b) Second Harmonic Signal vs. Concentration With Theoretical Approximation

### Other A-Band Transition Lines

The RQ(11,12) line was investigated primarily because it was a strong line and because it was convenient in the sense that it was easily accessed with the diode laser used in the experiment, and mode hopping of the diode laser was not a problem at the RQ(11,12) wavelength. Many lines in the Oxygen A-band were available for probing, and figures 8-11 show some of lines investigated.

Figure 8 shows the **first** derivative magnitude signal for the RQ(13,14) (760.258 nm) and the RR(11,11) (760.565 nm) Oxygen A-band transitions. Figure 9 shows the same transitions, but the signals show the magnitude of the **second** derivative.

In first derivative measurements, a signal offset is measured. This offset is due to the current ramp imposed on the laser diode. Recall that this ramp is used to sweep the laser wavelength across the absorption profile. As the current is increased, the desired effect is accomplished, but a resulting intensity ramp is also formed. When the first derivative is taken, the intensity slope appears as an offset. For higher order derivatives, there is no offset due to the fact that the second (or higher) derivative of a constant slope results in a zero.

Figure 10 shows the second derivative signals for the RR(13,13) (760.379 nm) and the RQ(11,12) (760.445nm). A laser mode hop was responsible for the break in the RQ (11,12) line at the end of the run. Figure 11 shows the second derivative signals for the RR(21,21) (759.859 nm) and the RQ(19,20) (759.831 nm) lines.

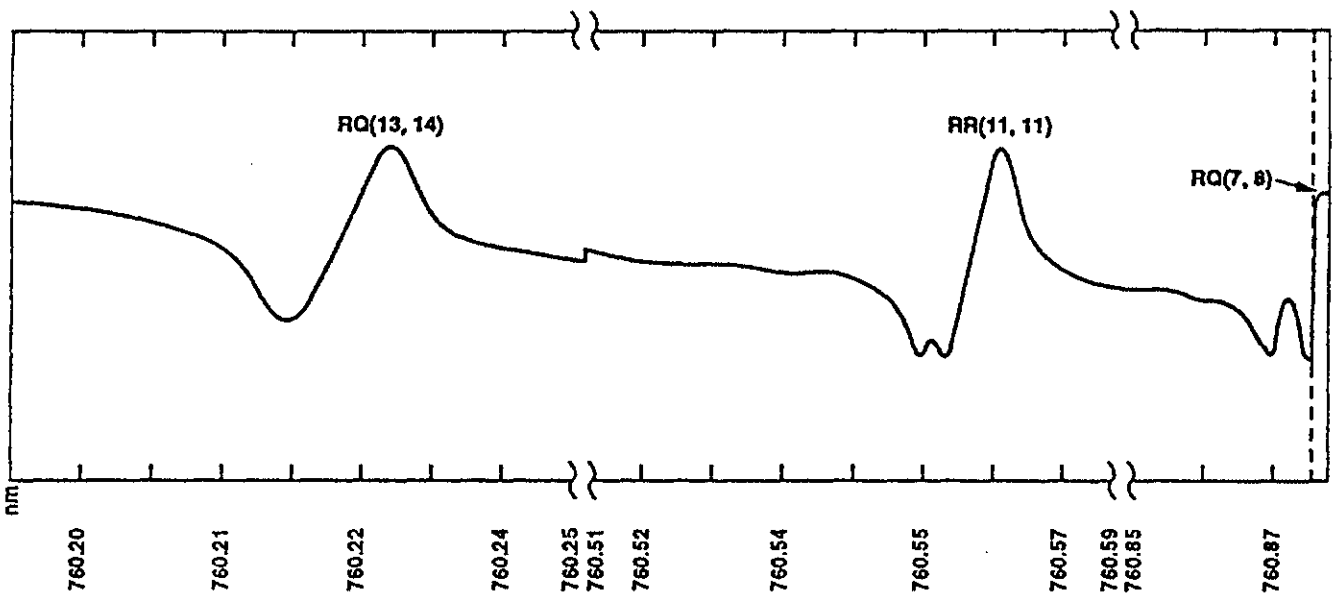


Figure 8 First Derivative Signal of Other A-Band Transitions

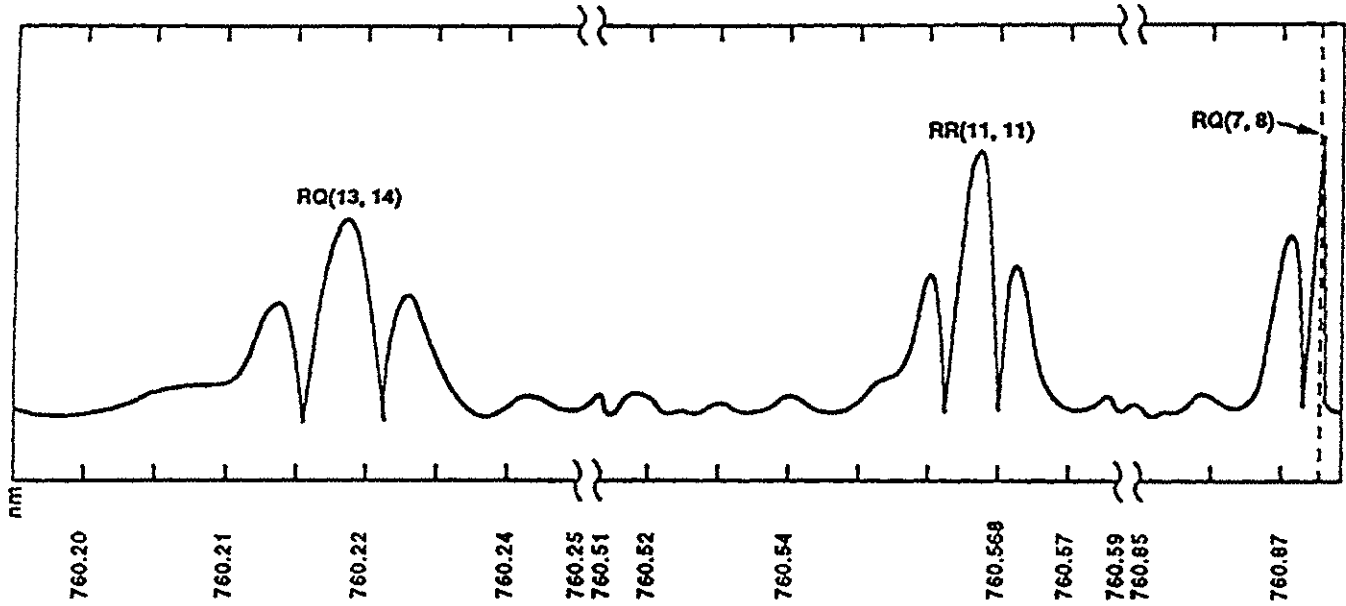
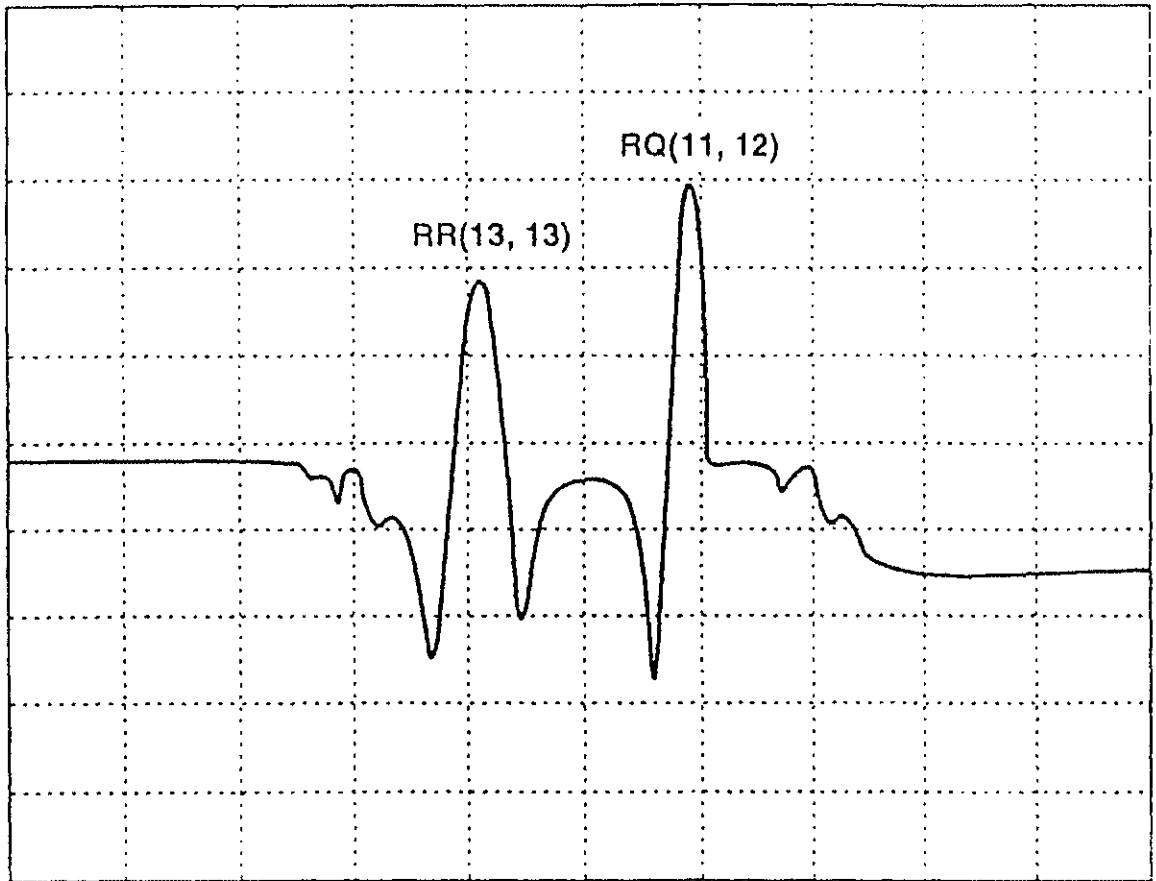


Figure 9 Second Derivative of Other A-Band Transitions



10 S /div

-2.375 S

Center = -1.151 e-6 ± 100.00 e-6 V

<b>Pause</b>		Ext S	Fr = 10.014 kHz			
		LOCK	Harmonic = 2		LOC	

Figure 10 Other A-Band Transitions

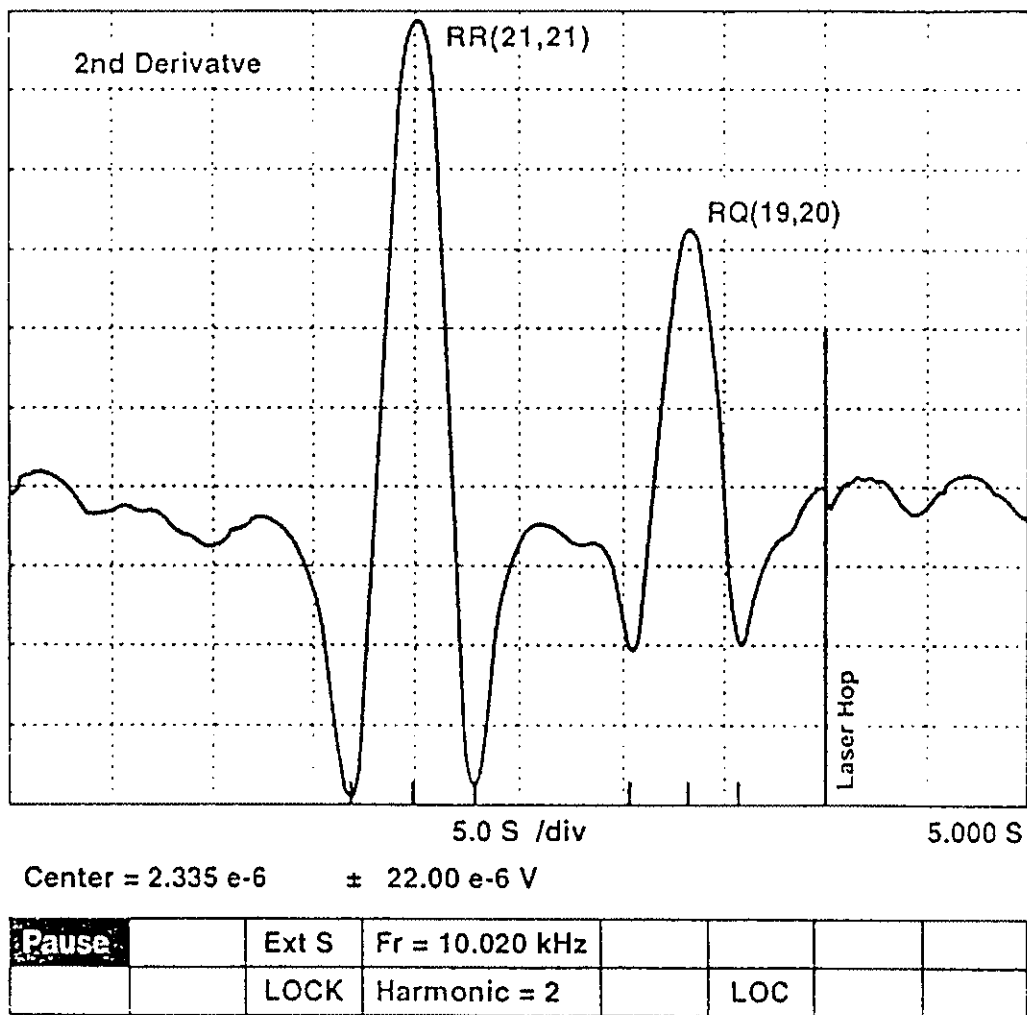


Figure 11 Other A-Band Transitions

## Temperature Measurements

As discussed above in Chapter II, a measurement of temperature can be performed by comparing the strengths of adjacent absorption lines. Figures 10 and 11 show a sample of some scans that were made of two adjacent transitions, performed at 300 K. From equation (41), and measured values of the relative line strengths (figure 11), we calculated  $(\Delta\omega_2/\Delta\omega_1) \approx 0.8$ . On the other hand, the experimentally measured values for the ratio of these linewidths is approximately 0.7. It is seen from equation (41) that an accurate measure of temperature requires a very careful measurement of the linewidths. In the experiments done in this work, the wavelength scale was obtained by monitoring the wavemeter readings. The latter, however, are updated every 500ms, causing an uncertainty in the linewidth measurements that account for the discrepancy between the two values above. To accurately measure temperature, a better method of measuring linewidths is required. More accurate temperature measurements would necessitate a much more accurate measurement of the linewidths than is currently possible.

## Higher Order Derivative Measurements

Several derivative order measurements were taken of the RQ(11,12) line. Since the bandwidth of the lock-in amplifier used in this experiment was limited to  $0 < h\omega_m \leq 100$  KHz, the modulation frequency was adjusted to comply with the limit. The first derivative measurement started with a modulation frequency of 25 kHz, and at the tenth derivative, a required decreased modulation frequency of 10 kHz was used.

Figures 12 and 13 show the actual derivative signals from the first derivative to the tenth derivative. The turning points of each derivative is indicated on each figure. From equations (28) and (29), it can be seen that for the Nth derivative of either the Gaussian or the Lorentzian, there are N+1 turning points. This is in agreement with the experimental data.

As seen in Chapter II, more detail about an absorption line is available as the derivative order is increased, but there is a trade off with signal strength. From equation (17), it is seen that the signal strength is diminished by  $\beta/2\omega_m$  for each increased derivative order. This is easily seen in figures 12 and 13.

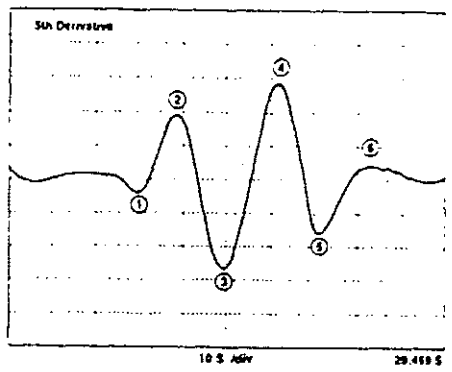
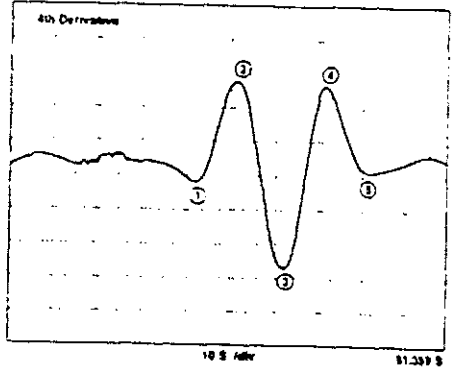
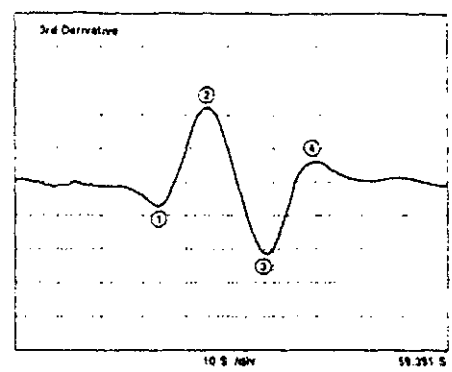
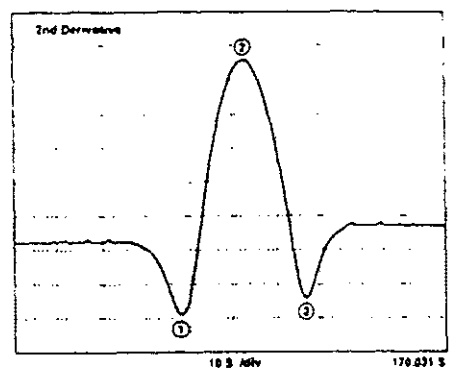
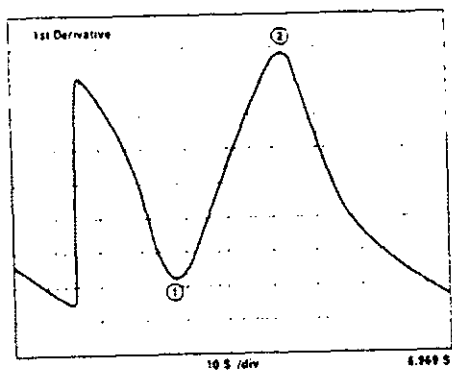


Figure 12 Derivative Signals

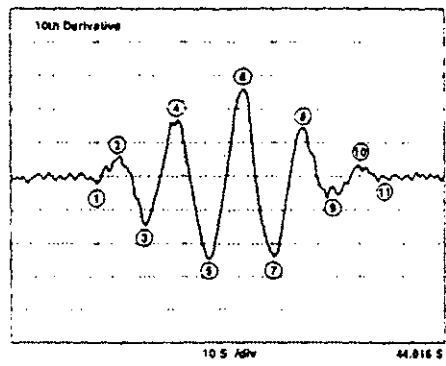
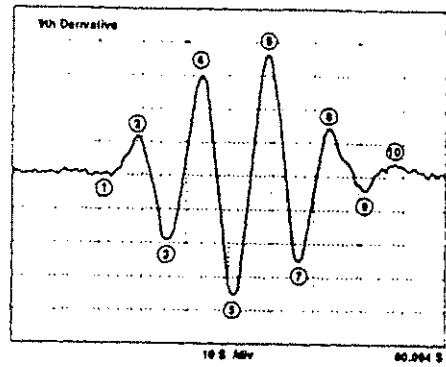
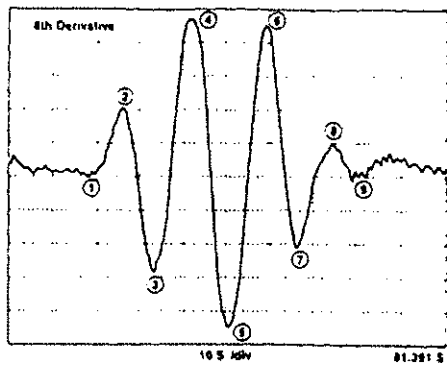
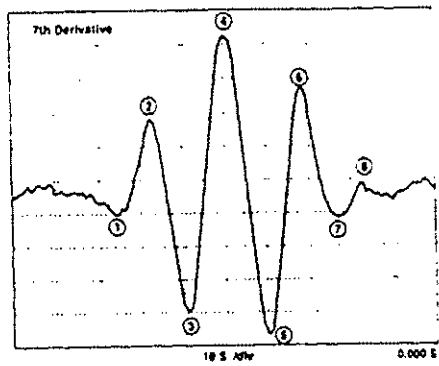
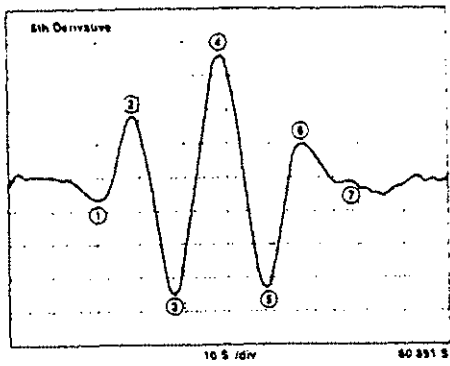


Figure 13 Derivative Signals

## Chapter IV.

### APPLICATIONS

#### Gas Concentration Measurements

Gas concentration monitoring is useful in many areas of science and industry.

The recent upgrading of EPA monitoring regulations, coupled with increasingly stringent emission requirements, has triggered a host of new applications for gas sensing [8]. One example is the stringent requirement to monitor  $\text{NO}_x$  emissions imposed on power plants. These power plants typically inject  $\text{NH}_3$  into the stack exhaust to curtail the  $\text{NO}_x$  emissions. In addition to monitoring the  $\text{NO}_x$  emissions, the power plants are required to monitor the  $\text{NH}_3$  levels. This monitoring can possibly be done with a derivative spectroscopy system non-intrusively and in real time.

Gas concentration measurements are also important in the monitoring of oxygen and other gasses used and produced in a combustion process. (It is clear that, in general, combustion diagnostics can be quite complicated and can involve the interaction of several different species, and it is possible that there may be species with partially overlapping spectra. Such an overlap would make the measurement of any one particular specie difficult; however we note that the Oxygen A band has a plethora of states that can be examined by the technique discussed. This allows the freedom to tune in to a region where interference from other species is minimal. Note

also that the method discussed in this work can be applied equally well, given the availability of the appropriate laser, to many other molecules involved in combustion (such as CO, CO<sub>2</sub>, H<sub>2</sub>O, etc.).

One example is in the NASA-Langley 8-ft wind tunnel. This tunnel is used in the scramjet engine experiments. The monitoring of oxygen in the tunnel may indicate the efficiency of the combustion process in the engine. If done in real time, fuel adjustments can be made during test runs, and if done in a non-intrusive fashion, wind tunnel flow dynamics will not be disturbed. It is hoped that the research done here will provide a foundation for such a system.

### **Temperature Measurements**

With the probing of two (or more) rovibronic transitions temperature information can be extracted. In extremely hot gasses, it may not be possible or wise to measure the temperature with an intrusive device. Using the method described here, temperature measurements can be made non-intrusively and at a safe distance. Temperature measurements for a host of applications are possible, including in the NASA-Langley wind tunnel mentioned previously. Temperature measurements can be made to measure burn efficiency in engines, furnaces, etc.

### **Velocity Measurements**

Many velocity measurements made in wind tunnels involve some sort of flow seeding with a fine dust. Techniques such as laser induced fluorescence measurements

are useful, but any time particulate matter is introduced in a wind tunnel environment, the possibility of damage to models or to the tunnel is present. Sand blasting is based on high speed particulate matter.

By measuring the Doppler shift distortions of an absorption profile, velocity information can be extracted [10]. This method provides a line integrated or averaged velocity measurement over the entire laser beam path length, but for many aerospace applications, a point velocity measurement is desired. One possible scheme to provide point velocity measurements incorporates the original modulated single mode diode laser with another saturating laser. The saturating laser is such that it will efficiently excite another transition in the probed molecules. By saturating a small part of the diode laser path length in pulses, the contribution from this segment will effectively be pulsed. By comparing a signal under saturation and an unperturbed signal, point velocity measurements may be extracted [11]. In this technique, one would perform a line-of-sight measurement in the usual fashion. In order to find the value of the parameter of interest at a particular position, a pulsed laser beam is focussed at this location. The pulsed laser is tuned to a strong absorption line, resulting in the saturation of this second transition. Such a saturation depletes the molecular density and therefore causes the line integrated signal to change. The value of the parameter at the location of interest can then be found from the difference in the two values of the line integrated absorption signals. Since the saturated segment is small, there may be some problems with signal strength, but by using stronger transitions, this scheme may prove to be feasible.

## Chapter V.

### CONCLUSION

Derivative absorption spectroscopy with tunable diode lasers provides a sensitive, non-intrusive technique for the gaseous measurement of specie type, density, temperature, velocity (by using Doppler shifts), and collisional cross-sections.

The Oxygen A-band transitions used in this research are spin forbidden and electric dipole forbidden, yet the transitions were probed, and information was easily extracted. This research has established that this technique is quite useful in the measurements of density, temperature and broadening mechanisms.

The ability to measure complete lineshape profiles allows the observation of lineshape distortions, especially in the wings, to be made. Hence, effects such as Dickie narrowing can be observed accurately. With higher order derivative spectroscopy, one can monitor lineshape features further and further into the lineshape wings, and lineshape anomalies can be seen. For example, it may be possible to distinguish between two nearly overlapping absorption profiles in an easy and convenient manner.

Possible applications include measurements in aerodynamics testing, combustion diagnostics and control, pollution monitoring and detection, and gaseous chemical kinetics, and because of the compact size and low power consumption of this

diode laser technology, diode laser spectroscopic techniques are ideal for space applications and other space and power limited environments.

Currently, most of the commercially available inexpensive (around \$25/laser diode) single mode diode lasers are produced for applications such as in CD players and bar code scanners. Although these diode lasers work well for these applications, they are not typically designed for spectroscopic work and due tend to mode hop and die prematurely. These trends are changing. With more and more scientific work being done with laser diodes, manufacturers are starting to provide reasonably priced single mode diode lasers built with the scientist in mind. Recently, at the Laser Applications to Chemical Analysis Conference sponsored by the Optical Society of America held in Jackson Hole, Wyoming, an entire segment of the conference was devoted to diode-laser based measurements and technology [8]. The advancement in laser diode technology will enable larger portions of the visible and near infrared spectrum to be accessed and will provide the spectroscopist access to more and more molecules and transitions.

## LIST OF REFERENCES

- [1] J. Reid and D. Labrie, Applied Physics B, **26**, pp. 203-210 (1981)
- [2] P. Milonni and J. Eberly, Lasers, Copyright 1988 by John Wiley & Sons, Inc., pp. 88-105.
- [3] From work done by Ying Lu, and Dr. A. N. Dharamsi at Old Dominion University. The expressions have been proved by induction.
- [4] M. Abramowitz and I. A. Stegun, The Handbook of Mathematical Functions, Volume 2, Dover Publishing, Dec. 1977, p. 360.
- [5] K. J. Ritter and T. D. Wilkerson, Journal of Molecular Spectroscopy, **121**, p. 1 (1987).
- [6] G. Herzberg, Molecular Spectra and Molecular Structure, I. Spectra of Diatomic Molecules, Second Edition, Sixth Printing, D. Van Nostrand Company, Inc. publishers, 1959, pp. 26, 124, 552, 560.
- [7] G. V. H. Wilson, Journal of Applied Physics, **34**, p. 3276 (1963).
- [8] 1994 Technical Digest Series Volume 5, Laser Applications to Chemical Analysis, sponsored by the Optical Society of America, pp. 75-96 (1994).
- [9] Joel Silver, 1994 Technical Digest Series Volume 5, Laser Applications to Chemical Analysis, sponsored by the Optical Society of America, p. 77 (1994).
- [10] L. C. Philippe and R. K. Hanson, Applied Optics, **32**, p. 6090 (1993).
- [11] A. N. Dharamsi and A. D. Jackson, in a paper to be published.
- [12] A. D. Jackson, A. N. Dharamsi and S. K. Chaturvedi, Laser Applications to Chemical Analysis, Technical Digest Volume 5, pp. 43-46.

- [13] From the Stanford Research Systems Model SR850 DSP Lock-in Amplifier operations manual, Copyright 1992 by Stanford Research Systems, Inc., p. 3-21.
- [14] L.S. Rothman, et al., Hitran Molecular Data Base, editions 1991, 1992, Vol. 48, p. 469.
- [15] Manuel Cardona, Modulation Spectroscopy, Academic Press (1964).